

# Phase-Coded Pulse Sequence for Passive Detection and Mapping of Ultrasound Cavitation

Shukuan Lu, Xianbo Yu, Renyan Li, Hongmei Zhang, and Mingxi Wan\*

*The Key Laboratory of Biomedical Information Engineering of Ministry of Education  
Department of Biomedical Engineering, School of Life Science and Technology, Xi'an Jiaotong University  
Xi'an, 710049, People's Republic of China  
<mailto: mxwan@mail.xjtu.edu.cn>*

**Abstract**—Focused ultrasound (FUS) therapy requires reliable and effective monitoring tools to understand the underlying physical mechanism, controlling the treatment process, and assessing the treatment effects. Passive acoustic mapping (PAM), extended from passive cavitation detection (PCD), can provide noninvasive real-time quantitative imaging associated with treatment effects, and has been widely used in more and more applications of ultrasound therapy. Most PAM applications are based on common one-dimensional arrays that are used for ultrasound diagnosis, assisting with the simplest time exposure acoustics algorithm. However, due to the limited frequency-dependent diffraction mode of these arrays, this algorithm results in a large point spread function (PSF). To address this challenge, in the present study, we proposed a phase-coded pulse sequence for FUS exposure to improve the PAM performance. In the experiments,  $K$  sinusoidal signals with equidistant phases were used to driven the FUS transducer, and a PCD transducer and a linear array were utilized to receive the acoustic emissions. The PCD signals of different phases were summed in time domain and then the spectrum analyses were performed, and the passive array signals were processed by a modified passive beamforming algorithm. *Ex vivo* experimental results illustrated that in PCD spectrum, the  $K$ -order and its integer harmonics were enhanced while the other harmonics were suppressed. The PAM results suggested that compared with single phase and pulse inversion, the PSF size was reduced by using 4-phase coding. This work may be beneficial to the accurate control of ultrasound treatment, particularly cavitation-mediated applications.

**Keywords**—ultrasound therapy monitoring; passive detection and mapping; phase-coded pulse sequence; point spread function

## I. INTRODUCTION

Over the past few years, focused ultrasound (FUS) has been proved to be effective in tumour thermal ablation, thrombolysis, and blood-brain barrier (BBB) opening [1–4]. Ultrasound therapy requires a reliable monitoring means to avoid the side effects on normal tissues. Magnetic resonance imaging can be applied in some therapy applications that are thermal in nature by detecting tissue temperature changes during the treatment process [5], but it is less efficient for some promising non-thermal cavitation-mediated applications (e.g., BBB opening). A commonly used ultrasound monitoring means in the past is passive cavitation detection (PCD) [6], which passively senses the acoustic emissions from cavitating bubbles with a single-element focused or unfocused transducer and then quantitatively analyse these signals to achieve the treatment evaluation. This technique has been employed to control the transcranial therapy in a close-loop manner [7]. The main

deficiency of PCD is the lack of spatial information of cavitation activity.

To compensate for the shortcoming of PCD, a multi-element array transducer can be applied for signal receiving during FUS exposure and then these signals are beamformed to obtained the spatial distribution of cavitation. This is the so-called PAM technique [8], which has played a key role in many ultrasound therapy applications since its birth. The most common PAM implementation is based on a delay-sum-integrate algorithm, e.g., time exposure acoustics [9], which yields a poor resolution when employing some narrow-aperture arrays that are used for ultrasound diagnosis. The reason behind this is that the size of the point spread function (PSF) of PAM is determined by the diffraction mode [10,11], in other words, it depends on the length of the transducer and the frequency of the signal of interest (or the receive bandwidth of the transducer).

Reducing PSF size by increasing the aperture of the diagnostic transducer may be very limited, because the aperture size can not be too large due to the diagnostic needs of the special parts of human body. However, we can consider how to increase the frequency to reduce the PSF size. The simplest way is to use a high-frequency transducer, but which is not suitable for clinical use because of limited imaging depth. Recently, pulse inversion technique, which has been used in ultrasound contrast imaging [12], was innovatively introduced in PAM to improve the detection sensitivity of transcranial cavitation [13]. By emitting two FUS pulses with inverse phases 0 and  $\pi$ , the nonlinear cavitation components were extracted while the linear components from skull or tissues were suppressed, therefore increasing the contrast-to-tissue ratio. On this basis, in this paper we proposed an improved FUS pulse design with the introduction of the phase-coded multi-pulse sequence, which has been proved to provide improved resolution and contrast for ultrasound tissue harmonic imaging [14,15]. What we demonstrate in this paper is that with the phase-coded multi-pulse sequence, high-frequency components in passive acoustic signals can be selectively enhanced and the reduced PSF size of PAM image can be obtained.

This paper is organized into four sections. Section II briefly reviews the phase-coded multi-pulse technique and describes the passive beamforming algorithm and the experimental settings. Section III presents the passive detection and mapping results of *ex vivo* experiments, accompanied our discussion. Finally, we concludes this paper in Section IV.

## II. METHODS

### A. Phase-coded Multi-pulse Technique

Assume that the FUS transducer is driven by  $K$  pulse signals whose phases are evenly spaced. The  $k$ th phase is

$$\varphi_k = \varphi_0 + \frac{2\pi k}{K}, \quad (1)$$

where  $k = 0, 1, \dots, K-1$ ,  $\varphi_0$  is the first phase.

The  $k$ th emitted pulse at the surface of the FUS transducer can be expressed as [14]

$$p_k(z=0, t) = P_0 \sin\left(\omega t + \varphi_0 + \frac{2\pi k}{K}\right), \quad (2)$$

where  $t$  denotes time,  $P_0$  is the peak negative pressure at the transducer surface, and  $\omega$  is the angular frequency.

At a specific distance  $z$  within the focal region, the pressure waveform corresponding to the  $k$ th emitted pulse signal can be written as [14]

$$p_k(z, t) = P_{fneg} \sum_{n=1}^{\infty} \frac{2J_n(nl_D)}{nl_D} \sin\left[n\left(\omega t + \varphi_0 + \frac{2\pi k}{K}\right)\right], \quad (3)$$

where  $P_{fneg} = gP_0$  is the focal peak negative pressure,  $g$  is the gain coefficient of the FUS transducer,  $l_D = \frac{\omega P_{fneg} z}{\rho c^3}$  is the dimensionless distance of the ultrasound propagation with  $\rho$  and  $c$  being the medium density and the sound speed in the medium, respectively,  $J_n(\alpha) = \sum_{m=0}^{\infty} \frac{(-1)^m (\alpha/2)^{2m+n}}{\Gamma(m+1)\Gamma(m+n+1)}$  corresponds to the  $n$ th harmonic with  $\Gamma(\cdot)$  denoting the Gamma function.

By summing  $K$  pressure waveforms in (3), the total pressure waveform at the given distance  $z$  can be obtained as follows [14]

$$p_s(z, t) = P_{fneg} \sum_{k=0}^{K-1} \sum_{n=1}^{\infty} \frac{2J_n(nl_D)}{nl_D} \sin\left[n\left(\omega t + \varphi_0 + \frac{2\pi k}{K}\right)\right]. \quad (4)$$

From (4), the  $n$ th harmonic component after summation can be extracted, as the following equation [14]

$$p_{s\_nth}(z, t) = P_{fneg} \sum_{k=0}^{K-1} \frac{2J_n(nl_D)}{nl_D} \sin\left[n\left(\omega t + \varphi_0 + \frac{2\pi k}{K}\right)\right]. \quad (5)$$

It can be seen from (5) that, when  $n$  is equal to  $K$  or its integer multiple,  $p_{s\_nth}(z, t) = KP_{fneg} \frac{2J_n(nl_D)}{nl_D} \sin(n\omega t + n\varphi_0)$ . Otherwise,  $p_{s\_nth}(z, t) = 0$ . This means that the  $K$ -order and its integer harmonics will be enhanced while the other harmonics will be suppressed.

### B. Modified Passive Beamforming Algorithm

Assume that the passive receiving array is an  $L$ -element linear array. The first step in the beamforming algorithm is to calculate the relative time delay [8]

$$\tau_j(\mathbf{x}) = \|\mathbf{x} - \mathbf{x}_j\| / c, \quad (6)$$

where  $\mathbf{x}$  and  $\mathbf{x}_j$  denote the spatial positions of the imaging point and the  $j$ th ( $j = 1, 2, \dots, L$ ) element, respectively.

The original signal received from the  $j$ th element under the  $k$ th phase,  $p_j^k(t)$ , is delayed according to the calculated delay in (6) and compensated with a factor  $\gamma_j(\mathbf{x}) = \|\mathbf{x} - \mathbf{x}_j\|^{1/2}$ , as the following equation [8]

$$s_j^k(\mathbf{x}, t) = \gamma_j(\mathbf{x}) p_j^k[t + \tau_j(\mathbf{x})]. \quad (7)$$

Then, the delay-compensate signals,  $s_j^k(\mathbf{x}, t)$ , are summed on the element dimension to give the beamformed signal of the  $k$ th phase

$$q^k(\mathbf{x}, t) = \sum_{j=1}^L s_j^k(\mathbf{x}, t). \quad (8)$$

The beamformed signals of  $K$  phases are further summed to give the final beamformed signal

$$q(\mathbf{x}, t) = \sum_{k=0}^{K-1} q^k(\mathbf{x}, t). \quad (9)$$

Finally, the square of the final beamformed output in (9) is integrated over a time period to calculate the source energy at a specific imaging point  $\mathbf{x}$

$$I(\mathbf{x}) = \frac{4\pi}{L^2 \rho c} \int_{T_1}^{T_2} q(\mathbf{x}, t)^2 dt, \quad (10)$$

where  $T_1$  and  $T_2$  represent the start time and the end time of signal acquisition.

According to (5), it is expected that the processing step in (9) will increase the  $K$ -order and its integer harmonic components. Therefore, the PSF size of PAM image will be reduced because it is frequency-dependent.

### C. Experimental Settings

The tissue samples used in the experiments were fresh *ex vivo* porcine muscles, which were purchased from the local supermarkets. As illustrated in Fig. 1(a), the experiments was carried out in a tank with deionized water. In order to avoid the possible ultrasonic reflection during the experiment, we placed the sound absorbing materials on the tank wall. A 1.2 MHz FUS transducer (Imasonic, Besancon, France) with a diameter of 156 mm and a focal size of 8 mm  $\times$  1.2 mm was used to induce acoustic cavitation activity inside the tissue samples. The FUS transducer was designed with a circular hole in the center to facilitate the use of a phased array or a single-element transducer for treatment monitoring. A wave generator (AWG420, Tektronix) emitted  $K$  sinusoidal pulse signals (duration = 10  $\mu$ s), as shown in Fig. 1(b), which were amplified

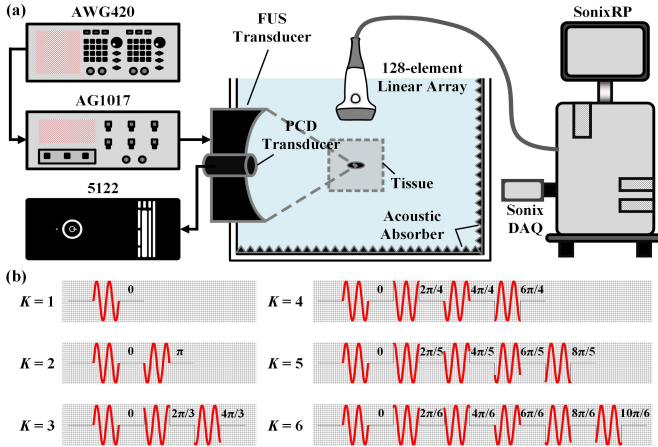


Fig. 1. (a) Experimental system setups. (b) FUS pulses with  $K$  equidistant phases ( $K = 1, 2, 3, 4, 5,$  and  $6$ ). An example of 2 cycles is given for clarity.

by a power amplifier (AG1017, T&C Power Conversion). Then, the amplified signals were fed into the FUS transducer. A single-element transducer with a bandwidth of 2.15–6.9 MHz (V309, Panametrics) was inserted into the center of the FUS transducer and used as the PCD transducer to receive the acoustic emissions under FUS pulses with different phases. These signals were collected by a high-speed acquisition card (5122, National Instruments) that had a 100-MHz bandwidth. The acoustic signals were also received by an L14–5/38 linear array that was mounted on an ultrasound imaging system (SonixRP, Ultrasonix), and collected by a parallel acquisition module (SonixDAQ, Ultrasonix) for further processing.

### III. RESULTS AND DISCUSSIONS

#### A. Passive Cavitation Detection

Fig. 2(a) plots the PCD signal in time domain when the FUS transducer is driven by 0-phase pulse (i.e., single phase) and the sum of PCD signals obtained when the FUS transducer is driven by two successive pulses with 0 phase and  $\pi$  phase (i.e., pulse inversion). As seen, the summed signal is significantly weaker than the signal of single phase. Fig. 2(b) plots the frequency spectra corresponding to the time-domain signals in Fig. 2(a). As seen, by using pulse inversion, the fundamental frequency and the odd harmonics are reduced while the even harmonics are retained, which is consistent with

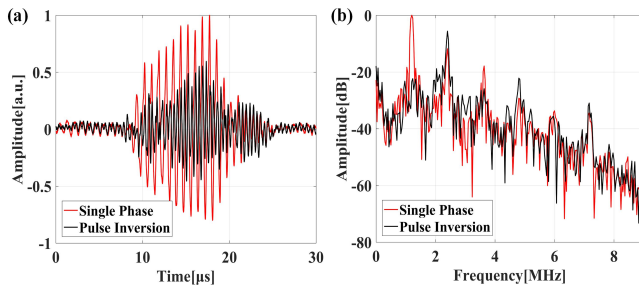


Fig. 2. (a) Time-domain PCD signals for FUS with 0-phase pulse (single phase) (red line) and the sum of PCD signals obtained by FUS pulses with 0 phase and  $\pi$  phase (pulse inversion) (black line). (b) Frequency spectra of time-domain PCD signals for FUS with single phase (red line) and pulse inversion (black line).

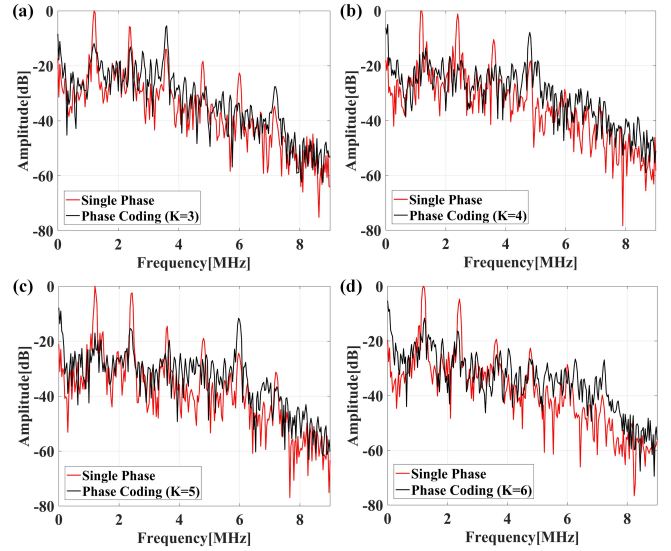


Fig. 3. Comparison of PCD frequency spectra between single phase (red lines) and phase coding with different phase number  $K$  (black lines): (a)  $K = 3$ , (b)  $K = 4$ , (c)  $K = 5$ , and (d)  $K = 6$ .

Pouliopoulos *et al.* work [13]. The statistical results indicate that compared with single phase, the 2nd harmonic (2.4 MHz), the 4th harmonic (4.8 MHz), and the 6th harmonic (7.2 MHz) are enhanced by  $5.70 \pm 0.91$  dB,  $5.93 \pm 1.21$  dB, and  $5.31 \pm 1.54$  dB, respectively.

The PCD signals obtained by FUS pulses with  $K$  equidistant phases are summed and the summed signal is analyzed in frequency domain. Fig. 3(a)–(d) plot the frequency spectra of phase coding with different phase number  $K$  (3, 4, 5, and 6). For comparison, the frequency spectrum in the single-phase case (0 phase) is also plotted in Fig. 3. It can be seen from Fig. 3(a) that in the signal summed from PCD signals of three equidistant phases, the 3rd harmonic (3.6 MHz) and the 6th harmonic (7.2 MHz) are enhanced, while other harmonics are suppressed. The statistical results show that compared with the case of single phase, the enhancements are  $8.55 \pm 1.04$  dB and  $7.75 \pm 1.51$  dB for the 3rd and 6th harmonics, respectively. Also, the 4th harmonic, the 5th harmonic (6.0 MHz), and the 6th harmonic are obviously enhanced in the cases of 4-phase coding, 5-phase coding, and 6-phase coding, as shown in Figs. 3(b)–(d). Compared with the single-phase case, the enhancements of the 4th to 6th harmonic components are  $10.65 \pm 2.27$  dB,  $12.54 \pm 0.54$  dB, and  $14.37 \pm 4.07$  dB, respectively. The above results indicate that by modulating the emitting phase of FUS pulses, the desired harmonic components can be selectively enhanced.

#### B. Passive Acoustic Mapping

The PAM images obtained by FUS with single phase (i.e., 0 phase), pulse inversion and phase coding ( $K = 4$ ) are displayed in Fig. 4(a)–(c), respectively, with a logarithmic scale. Fig. 4(a) is created by the conventional algorithm (i.e., time exposure acoustics), and Fig. 4(b) and (c) are created using the modified passive beamforming algorithm illustrated in Section II-B. The PSF size of the PAM image is quantified by the  $A_{50}$  area [16]. From the result of single phase shown in

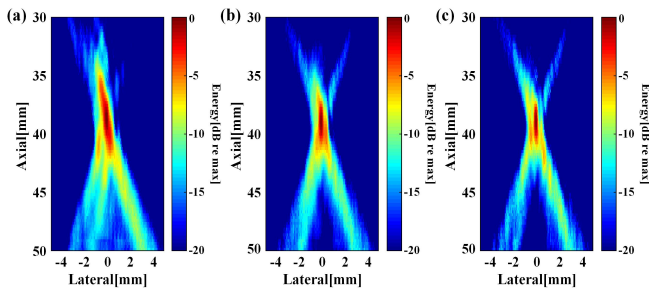


Fig. 4. PAM images obtained by FUS with (a) single phase, (b) pulse inversion, and (c) phase coding ( $K = 4$ ). All PAM images are shown with a 20 dB dynamic range.

Fig. 4(a), it can be seen that there is a significant X-type tail artifacts in the image, which yields a large PSF and seriously degrades the image quality. The main reason is the diffraction mode of the linear array is limited [11]. As shown in Fig. 4(b), due to that the fundamental and odd harmonics have been suppressed by pulse inversion, a better PAM image with a smaller bright spot in the center is obtained. The PSF size is decreased by 34.75% when compared with single phase. Thanks to the enhanced 4th harmonic by 4-phase coding of FUS pulses, the image quality is further improved [Fig. 4(c)]. The PSF size is further decreased by 40.65% on the basis of pulse inversion. Although the PSF can be decreased, it is seen from Fig. 4(c) that the phase-coded multi-pulse technique still can not eliminate the non-symmetric X-artifacts. The attribution to the non-symmetric artifacts may be the defects of the receiving array and variable sound speed in the medium, which may be resolved by some adaptive passive beamforming algorithms [17,18].

Due to the strong attenuation of high-frequency ultrasound signal by the skull occlusion, the resolution performance of transcranial PAM is limited. It can be expected that the phase-coded multi-pulse technique in this paper can be used to improve the detectability of transcranial PAM. It should also be noted that the phase-coded multi-pulse technique can not only be used in two-dimensional PAM based on a linear array, but also in three-dimensional PAM with an area array or a hemispherical array.

#### IV. CONCLUSION

In the present study, the phase-coded multi-pulse technique that has been used in ultrasound tissue harmonic imaging was proposed for passive detection and mapping of acoustic emissions during FUS exposure. The experimental results showed that after summing the PCD signals obtained by FUS pulses with  $K$  equidistant phases, the harmonics components can be selectively enhanced. Also, using 4-phase coding can reduce the  $A_{50}$  area of PAM image in comparison with both single phase and pulse inversion, therefore a smaller PSF can be obtained. Future work will combine this technique with the adaptive beamforming algorithm to achieve better PAM performance and validate it by *in vivo* experiments.

#### ACKNOWLEDGMENT

This work was supported by the National Natural Science Foundation of China (Grant Nos. 11904280 and 81827801), Project funded by China Postdoctoral Science Foundation (No. 2018M640996), and the National Natural Science Foundation of China (Grant Nos. 81771854, 11874049, and 11474229).

#### REFERENCES

- [1] J. E. Kennedy, "High-intensity focused ultrasound in the treatment of solid tumours," *Nat. Rev. Cancer*, vol. 5, no. 4, pp. 321–327, 2015.
- [2] N. McDannold, G. T. Clement, P. Black, F. Jolesz, and K. Hynynen, "Transcranial magnetic resonance imaging-guided focused ultrasound surgery of brain tumors: Initial findings in 3 patients," *Neurosurgery*, vol. 66, no. 2, pp. 323–332, 2010.
- [3] R. Medel, R. W. Crowley, M. S. McKisic, A. S. Dumont, and N. F. Kassell, "Sonothrombolysis: An emerging modality for the management of stroke," *Neurosurgery*, vol. 65, no. 5, pp. 979–993, 2009.
- [4] N. McDannold, C. D. Arvanitis, N. Vykhodtseva, and M. S. Livingstone, "Temporary disruption of the blood-brain barrier by use of ultrasound and microbubbles: Safety and efficacy evaluation in rhesus macaques," *Cancer Res.*, vol. 72, no. 14, pp. 3652–3663, 2012.
- [5] K. Hynynen, "MRIGHIFU: A tool for image-guided therapeutics," *J. Magn. Reson. Imaging*, vol. 34, no. 3, pp. 482–493, 2011.
- [6] T. Li *et al.*, "Passive cavitation detection during pulsed HIFU exposures of ex vivo tissues and in vivo mouse pancreatic tumors," *Ultrasound Med. Biol.*, vol. 40, no. 7, pp. 1523–1534, 2014.
- [7] T. Sun *et al.*, "Closed-loop control of targeted ultrasound drug delivery across the blood-brain/tumor barriers in a rat glioma model," *Proc. Natl. Acad. Sci. U. S. A.*, vol. 114, no. 48, pp. E10281–E10290, 2017.
- [8] M. Gyöngy and C. C. Coussios, "Passive spatial mapping of inertial cavitation during HIFU exposure," *IEEE Trans. Biomed. Eng.*, vol. 57, no. 1, pp. 48–56, 2010.
- [9] S. Norton and I. J. Won, "Time exposure acoustics," *IEEE Trans. Geosci. Remote Sens.*, vol. 38, no. 3, pp. 1337–1343, 2000.
- [10] K. J. Haworth *et al.*, "Passive imaging with pulsed ultrasound insonations," *J. Acoust. Soc. Amer.*, vol. 132, no. 1, pp. 544–553, 2012.
- [11] K. J. Haworth, K. B. Bader, K. T. Rich, C. K. Holland, and T. D. Mast, "Quantitative frequency-domain passive cavitation imaging," *IEEE Trans. Ultrason. Ferroelectr. Freq. Control*, vol. 64, no. 1, pp. 177–191, 2017.
- [12] D. H. Simpson, C. T. Chin, and P. N. Burns, "Pulse inversion Doppler: a new method for detecting nonlinear echoes from microbubble contrast agents," *IEEE Trans. Ultrason. Ferroelectr. Freq. Control*, vol. 46, no. 2, pp. 372–382, 1999.
- [13] A. N. Poulipoulos, M. T. Burgess, and E. E. Konofagou, "Pulse inversion enhances the passive mapping of microbubble-based ultrasound therapy," *Appl. Phys. Lett.*, vol. 113, no. 4, pp. 044102, 2018.
- [14] Q. Ma, D. Zhang, X. Gong, and Y. Ma, "Phase-coded multi-pulse technique for ultrasonic high-order harmonic imaging of biological tissues in vitro," *Phys. Med. Biol.*, vol. 52, no. 7, pp. 1879–1892, 2007.
- [15] W. Wilkening, M. Krueger, and H. Ermert, "Phase-coded pulse sequence for non-linear imaging," in *Proc. IEEE Ultrason. Symp.*, 2000, pp. 1559–1562.
- [16] S. H. Abadi, K. J. Haworth, K. P. Mercado-Shekhar, and D. R. Dowling, "Frequency-sum beamforming for passive cavitation imaging," *J. Acoust. Soc. Amer.*, vol. 144, no. 1, pp. 198–209, 2018.
- [17] C. Coviello *et al.*, "Passive acoustic mapping utilizing optimal beamforming in ultrasound therapy monitoring," *J. Acoust. Soc. Amer.*, vol. 137, no. 5, pp. 2573–2585, 2015.
- [18] S. Lu *et al.*, "Passive acoustic mapping of cavitation using eigenspace-based robust Capon beamformer in ultrasound therapy," *Ultrason. Sonochem.*, vol. 41, pp. 670–679, 2018.